Photoacoustics 38 (2024) 100625

Contents lists available at ScienceDirect

Photoacoustics

journal homepage: www.elsevier.com/locate/pacs

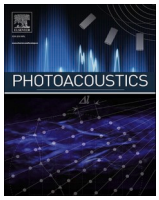

No document header

Effect of gas turbulence in quartz-enhanced photoacoustic spectroscopy: A comprehensive flow field analysis

Andrea Zifarelli [a,b], Giuseppe Negro [c], Lavinia A. Mongelli [b], Angelo Sampaolo [a,b], Ezio Ranieri [d], Lei Dong [a,d], Hongpeng Wu [a,d,*], Pietro Patimisco [a,b,*], Giuseppe Gonnella [c], Vincenzo Spagnolo [a,b]

[a] State Key Laboratory of Quantum Optics and Quantum Optics Devices, Institute of Laser Spectroscopy, Shanxi University, Taiyuan 030006, China
[b] PolySense Lab-Dipartimento Interateneo di Fisica, Politecnico and University of Bari, Via Amendola 173, Bari I-70126, Italy
[c] Dipartimento di Fisica, Università Degli Studi di Bari and INFN, Sezione di Bari, via Amendola 173, Bari I-70126, Italy
[d] Collaborative Innovation Center of Extreme Optics, Shanxi University, Taiyuan 030006, China

ARTICLE INFO

Keywords:
QEPAS
Flow field analysis
Turbulence effect
Photoacoustic wave generation

ABSTRACT

Here we present a computational and experimental fluid dynamics study for the characterization of the flow field within the gas chamber of a Quartz-Enhanced Photoacoustic Spectroscopy (QEPAS) sensor, at different flow rates at the inlet of the chamber. The transition from laminar to turbulent regime is ruled both by the inlet flow conditions and dimension of the gas chamber. The study shows how the distribution of the flow field in the chamber can influence the QEPAS sensor sensitivity, at different operating pressures. When turbulences and eddies are generated within the gas chamber, the efficiency of photoacoustic generation is significantly altered.

1. Introduction

The detection of gas species with high precision holds significant importance in various scientific and industrial domains. This capability is instrumental in enhancing scientific comprehension and surveillance across a diverse spectrum of applications, including but not limited to environmental monitoring [1,2], industrial process control analysis [3,4], combustion processes [5,6], as well as breath analysis for medical studies [7,8]. On the one hand gas sensors based on spectroscopic techniques have demonstrated high and satisfying capability for adapting at different applications [9–12], but on the other hand further analysis are still needed for studying and modeling the impact of thermo- and fluid-dynamic properties of the gas mixture on the sensing performance, with potential further limitations to be considered in the range of sensor operability.

In a typical optical gas sensor operating in flow regime, the gas is injected into a volume chamber by means of an inlet at low flow rates, typically < 100 standard cubic centimeters (sccm). The inlet has a radius much smaller than the transverse dimension of the gas chamber. Thus, the gas expands in the chamber before being expelled through an outlet connected to a pump. As a result, the steady-state spatial distribution of molecules in the chamber can be related to a complex and disordered dynamical behavior. By changing some parameters, such as inlet and outlet conditions and geometry/dimension of the gas chamber, the flow can undergo a transition from stable and laminar to turbulent regime. The transition from laminar to turbulent flow mode is correlated to Reynolds number [13,14]. Laminar case is ruled by slow speeds: fluid flows regularly, smoothly and in parallel layers without any disruption. The motion of fluids becomes turbulent as the velocity field magnitude increases: the fluid is disordered, chaotic and layers start mixing with each other [15].

In direct absorption spectroscopy techniques, the photodetector is placed outside the gas chamber, thus the flow distribution within it does not play a crucial role. Light is absorbed along the pathway within the chamber and the detector collects the light at the exit [16]. The sensing mechanism differs when exploiting indirect absorption spectroscopy techniques. In this case, the non-radiative energy relaxation of optically excited molecules gives rise to both local thermal diffusion and acoustic wave propagation, and a detector is directly placed within the gas chamber to locally probe one of the two effects. An arm of a Mach-Zender interferometer is immersed in the gas cell to locally detect the thermal diffusion in photothermal spectroscopy [17,18]; a

* Corresponding authors at: State Key Laboratory of Quantum Optics and Quantum Optics Devices, Institute of Laser Spectroscopy, Shanxi University, Taiyuan 030006, China
E-mail addresses: wuhp@sxu.edu.cn (H. Wu), pietro.patimisco@uniba.it (P. Patimisco).

https://doi.org/10.1016/j.pacs.2024.100625
Received 16 April 2024; Received in revised form 31 May 2024; Accepted 2 June 2024
Available online 10 June 2024

microphone, a cantilever and a spectrophone (composed by a quartz tuning fork and a pair of resonator tubes) are used in standard photoacoustic spectroscopy (PAS) [19,20], cantilever-enhanced photoacoustic spectroscopy (CEPAS) [21–23], and quartz-enhanced photoacoustic spectroscopy (QEPAS) [24–26], respectively, to detect the sound waves that propagate within the gas cell. While in PAS the geometry of the gas chamber must match – in the easiest configuration– a Helmholtz acoustic resonator with the microphone placed at the antinode point of the fundamental longitudinal mode of the standing wave pattern, in QEPAS and CEPAS the gas chamber design is more flexible and subject to less constraints. Chambers can be constructed of various materials and dimensions since they serve only for isolating the gas mixture to be analyzed from the external environment. It goes without saying that any deviation of the flow regime within the chamber from the laminar one can impact on the detection of the spectrophone or the cantilever: acting as point detector, they are affected by the degree of disorder, no-uniformity and chaoticity of the flow field inside the chamber.

In this paper we investigated how changes in the flow mode from laminar to turbulent influence the photoacoustic detection when the flow rate is increased in a QEPAS gas chamber. A QEPAS sensor for methane detection was designed with the possibility of interchanging three different-in-size gas chambers for investigating both the laminar and turbulent regime without altering the sensor architecture. The study is described in two sections: (i) computational analysis of the flow field in the gas chamber, around the spectrophone; and (ii) experimental analysis of the QEPAS signal at different flow rates, at three operating pressures.

2. Definition of the geometry and selection of parameters for the analysis

Starting from the CAD of the acoustic detection module ADM01 (Fig. 1a) provided by Thorlabs GmbH [27], the computational domain of the internal module chamber (Fig. 1b) has been preliminary reconstructed with a volume extraction technique implemented in the Ansys Fluent Reclaim Volume software.

To study the role of the geometry on the flow field distribution, starting from the volume reconstruction of ADM01 two additional gas chambers were designed. First, a gas chamber with higher volume named hereafter as ADM02, was designed with inlet and outlet placed at the same distance from the bottom and top wall (Fig. 2a). The reason for this slight modification of ADM01 geometry will be clarified later. Fig. 2b shows the computational mesh of the empty volume chamber of ADM02. Then, a smaller ADM usually employed with standard 32.7 kHz-QTF, named hereafter as ADM03, with internal volume chamber depicted in Fig. 2c was also designed.

For the analysis of all three volume chambers, the computational meshes were created by discretizing the computational domain. Care was required for discretization of both the inlet and outlet regions and on the upper boundary of the chamber: the presence of steps requires a significant increase of the local density of discretized cells to avoid spurious numerical effects. The fluid considered for the simulation is air, with density $\rho = 1.225\ \mathrm{kg/m^3}$ and viscosity $\mu = 1.789{\cdot}10^{-5}$ kg/m·s. Under these conditions, the isothermal incompressible numerical solver was used in the Ansys Fluent Fluid Solver Software, imposing that the characteristic velocity of the problem is much lower than the characteristic sound velocity. The software solves the continuity and momentum equation of the fluid within a fixed volume with the Volume of Fluid Method (VFM) numerical method.

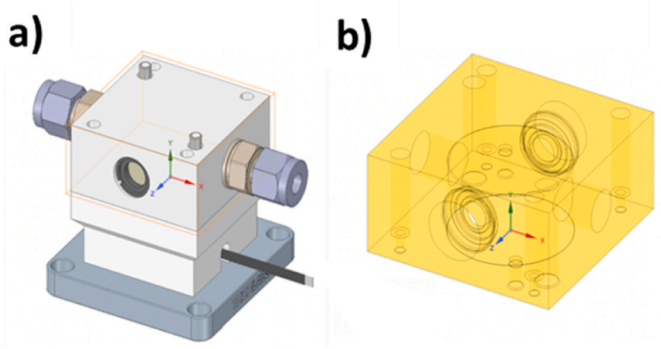

Fig. 1. (a) CAD of the starting acoustic detection module ADM01; (b) reconstruction of the internal volume chamber.

After solution convergence, the results were discussed in terms of the velocity field inside the volume and at the boundaries. As a measure of the chaoticity or irregularity of the flow, both the turbulent intensity and the turbulent viscosity were considered for identifying regions where the flow is more disordered and thus supposed to affect the efficiency of the photoacoustic detection when a spectrophone is placed in the chamber. Turbulence intensity is defined as the ratio of standard deviation of fluctuating flow velocity to the mean flow speed, and it represents the intensity of flow velocity fluctuations. Turbulent viscosity is the proportionality factor describing the turbulent transfer of energy because of moving eddies, giving rise to tangential stresses. In the following section, the flow behavior inside the chamber will be analyzed at different mass flow rates (MFRs).

3. Injection conditions of the gas within the volume chamber

Before entering in the chamber, the gas passes through a cylindrical, metallic, or plastic pipe. Within the pipe, the Mass Flow Rate (MFR) passing through pipe with a circular cross-section S in time t, is related to the velocity v by the following expression:

$$MFR = S \bullet v \tag{1}$$

Looking at the Reynolds number, one can determine whether the gas in a cylindrical pipe will flow in the laminar or turbulent regime. Indeed, the Reynolds number is typically defined in terms of the cross-sectional geometry of the pipe as:

$$\mathrm{Re} = \frac{\rho v D}{\mu} \tag{2}$$

In the present investigation, different MFRs were investigated with an upper limit of 500 sccm, which was considerably beyond the typical operating flow rate for QEPAS sensors. Considering the selected tube diameter $D = 6$ mm and with the air as gas carrier, the Reynolds number reaches a value lower than 20 in the case of highest flow rate. Thus, the fluid flow can be reasonably assumed to be laminar within tubes before entering in the chamber. This is the starting point of the simulation: a laminar fluid with a fixed MFR is injected into the chamber inlet.

Additional starting conditions for the simulation are given by the typical settings for QEPAS sensors' operation. The pressure drop between the inlet and outlet of the volume chamber is fixed to zero because of a pressure controller and a pump both located downstream, as schematically represented in Fig. 3.

Therefore, once the stationary regime is achieved the pressure setpoint (typically below the atmospheric pressure) reached, this value is homogeneous in the whole gas chamber and also the total flow is constant along the whole gas delivery line.

4. Simulation results

The analysis of the flow properties was performed without any optomechanical component, threating the chamber normally accommodating the spectrophone as an empty volume.

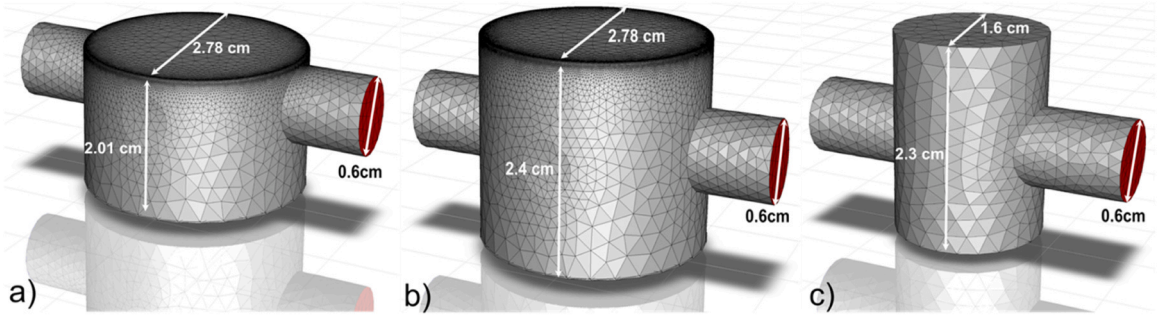

Fig. 2. Computational mesh of the internal volume chamber of ADM01 (a), ADM02 (b), and ADM03 (c). Inlet and outlet have the same dimensions in all the three geometries.

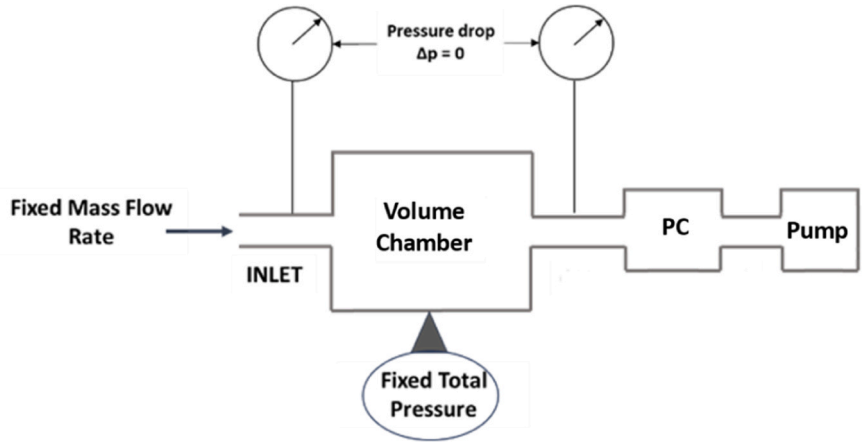

Fig. 3. Schematic of the operating condition of a gas chamber in a QEPAS sensor. An upstream mass flow controller fixes the flow rate injected in the chamber while a pressure controller and a pump both located downstream regulate the pressure within the volume chamber. PC – Pressure Controller.

4.1. Analysis of ADM01

Fig. 4 shows the velocity field on a plane parallel to inlet and outlet as well as the velocity streamlines, for three different values of MFR, namely 50 sccm (Fig. 4a and 4b), 100 sccm (Fig. 4c and 4d) and 500 sccm (Fig. 4e and 4f). Fig. 4a, 4c and 4e are top views; Fig. 4b, 4d and 4f are in perspectives.

At MFR = 50 sccm, the flow is clearly laminar (Fig. 4a and 4b). The fluid flows in parallel layers, with no significant disruption between the layers. In this regime, the fluid tends to flow without lateral mixing, and adjacent layers slide past one another. This would correspond to the perfect working conditions for a QEPAS volume chamber, characterized by an intense flow concentrated at the center of the chamber (named hereafter as mainstream) and investing the sensitive element, with a small expansion from the center characterized by homogenous variations. Increasing the MFR to 100 sccm (Fig. 4c and 4d), the fluid does not flow in parallel layers, and disruptions between the layers appear. This is due to the appearance of vortices near the inlet region (clearly visible in Fig. 4d). At 500 sccm (Fig. 4e and 4f), the presence of vortices both on the right and left of the mainstream is more pronounced. Moreover, the vortices are not completely developed on planes parallel to the mainstream. These structures strongly affect the flow field in the mainstream.

Fig. 5a and 5d show the velocity magnitude on a plane cutting the center of the chamber and perpendicular to inlet and outlet at 50 sccm and 500 sccm, respectively. The center of the plane corresponds to the position where the spectrophone is supposed to be placed. At 50 sccm, the flow field magnitude is quite symmetric and homogenous (Fig. 5a); at 500 sccm, it appears to be deformed, due to the presence of the vortices (Fig. 5d). It is also worth noticing that in this case two spots appear near the bottom wall, on the two bottom corners, identified as dead volumes for the flow. Dead volumes can be represented as unmoving, stagnant, and residual localized spaces within the gas chamber that can act either as reservoir for heavy or sticky molecules or as low-density space. In both cases, dead volumes represent an issue for a QEPAS sensor operation. The slow trapping or releasing molecules can lead to drifts in the actual number of absorbing molecules that hits the spectrophone, thus affecting the accuracy of the concentration measurement. The same considerations can be done by considering the velocity magnitude on a plane parallel to the inlet and outlet, at 50 sccm (Fig. 5b) and 500 sccm (Fig. 5e). At 500 sccm, the flow intensity significantly widens and spread from the mainstream with respect to a low flow rate of 50 sccm. An analysis of the turbulent intensity was also performed at 50 sccm and 500 sccm (Fig. 5c and 5f).

No turbulent intensity is present at 50 sccm (Fig. 5c). At 500 sccm, the turbulent intensity is highly inhomogeneous, with a high turbulent intensity fully developed inside the chamber (Fig. 5f). The turbulent viscosity is now highly significant, clearly indicating the existence of different fluid layers flowing with different viscosity.

4.2. Analysis of ADM02

To study the role of the geometry on the flow field distribution and on the vortices' formation at 500 sccm, ADM02 was designed starting from ADM01 geometry, with inlet and outlet placed at the same distance from the bottom and top wall (see Fig. 2b). The idea comes from the supposition that both the inlet and outlet are too close to the top wall, creating a strong interaction of the flow field with the top wall. This can cause the formation of incomplete vortices with consequent distortion of the streamlines (Fig. 4d and 4f). Fig. 6a-d presents the results of the simulation for the highest value of MFR considered, namely 500 sccm,

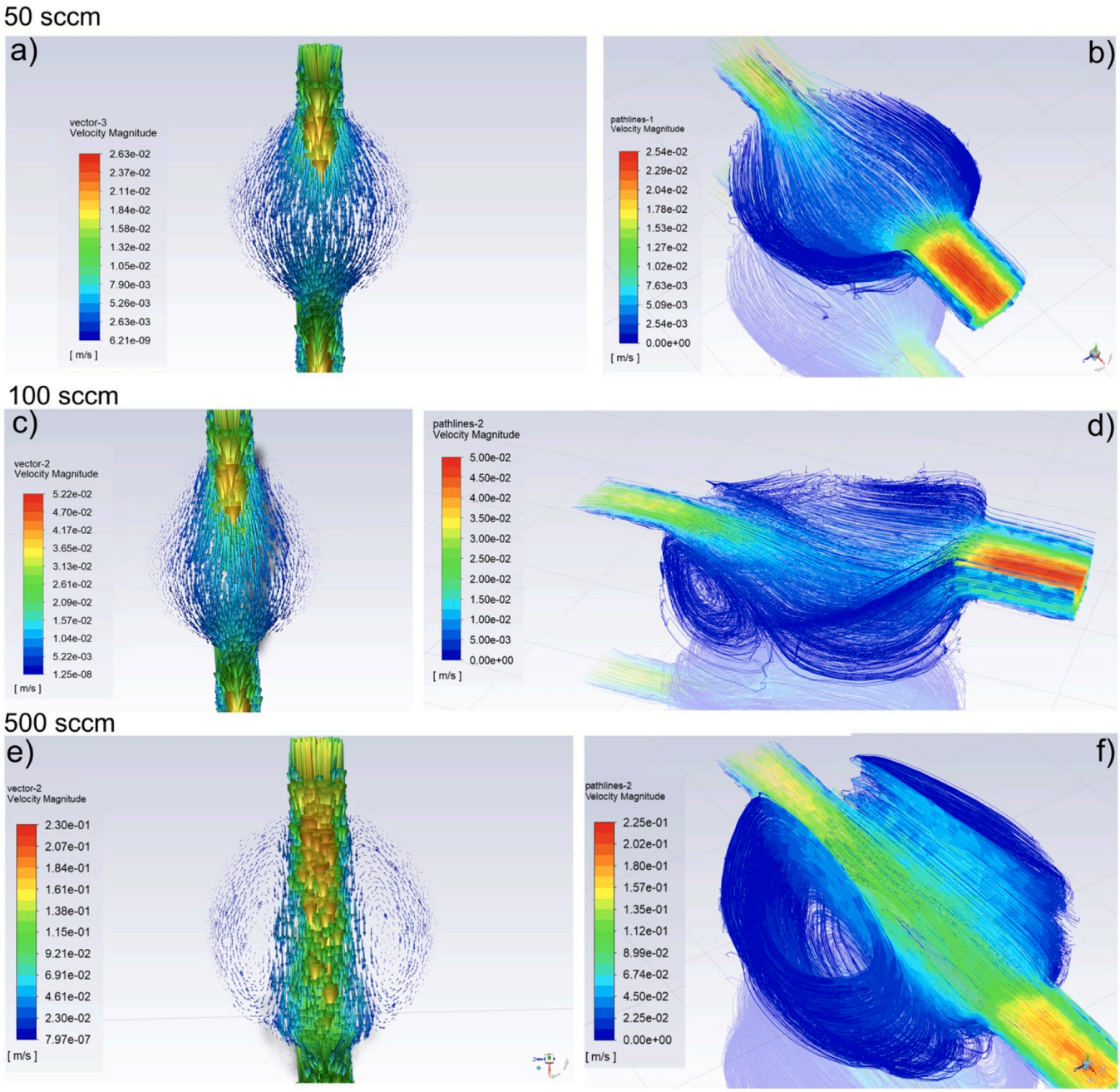

Fig. 4. Flow Field analysis within the empty volume chamber at 50 sccm ((a) and (b)), 100 sccm ((c) and (d)) and 500 sccm ((e) and (f)).

for ADM02.

Fig. 6a show the flow field at the center of the chamber. While it is still characterized by the presence of two vortices at the right and left side of the mainstream, a quick comparison with Fig. 4f suggests that in this case they are fully developed on the plane. The symmetry imposed by the geometry of the chamber ensures that the centers of the vortices lay on a plane parallel to the walls. This has an important consequence on the flow configuration. The mainstream (Fig. 6c) has now a more symmetric shape with no expansion zones (to be compared with Fig. 5e). We can argue this because the flow is fully developed on the center plane of the device: vortices lie on the same plane of the mainstream and are completely formed, thus the molecules are reintroduced in the mainstream and can reinforce it on this plane. However, four dead zones in the corners are still present, as observed in Fig. 6b, due to the expansion of vortices out of the mainstream plane. The analysis of the turbulent intensity and viscosity is displayed in Fig. 6d, further confirming the overall increase of the homogeneity and symmetry of the flow for this geometry.

4.3. Analysis of ADM03

To prevent the formation of vortices, the ADM03 with a significant smaller volume with respect to ADM01 and ADM02 was also considered. Fig. 7 shows the velocity field on a plane parallel to inlet and outlet as well as the velocity streamlines, for three different values of flow rate, namely 50 sccm (Fig. 7a and 7b), 100 sccm (Fig. 7c and 7d)), and 500 sccm (Fig. 7g and 7h).

The velocity field clearly shows a consistent flow condition across all the values of MFRs considered. The reduced radius of the chamber inhibits the formation of lateral vortices found for ADM01 and ADM02. The velocity streamlines, on the other hand, show another important feature of the updated geometry. At 50 sccm, streamlines expand in the

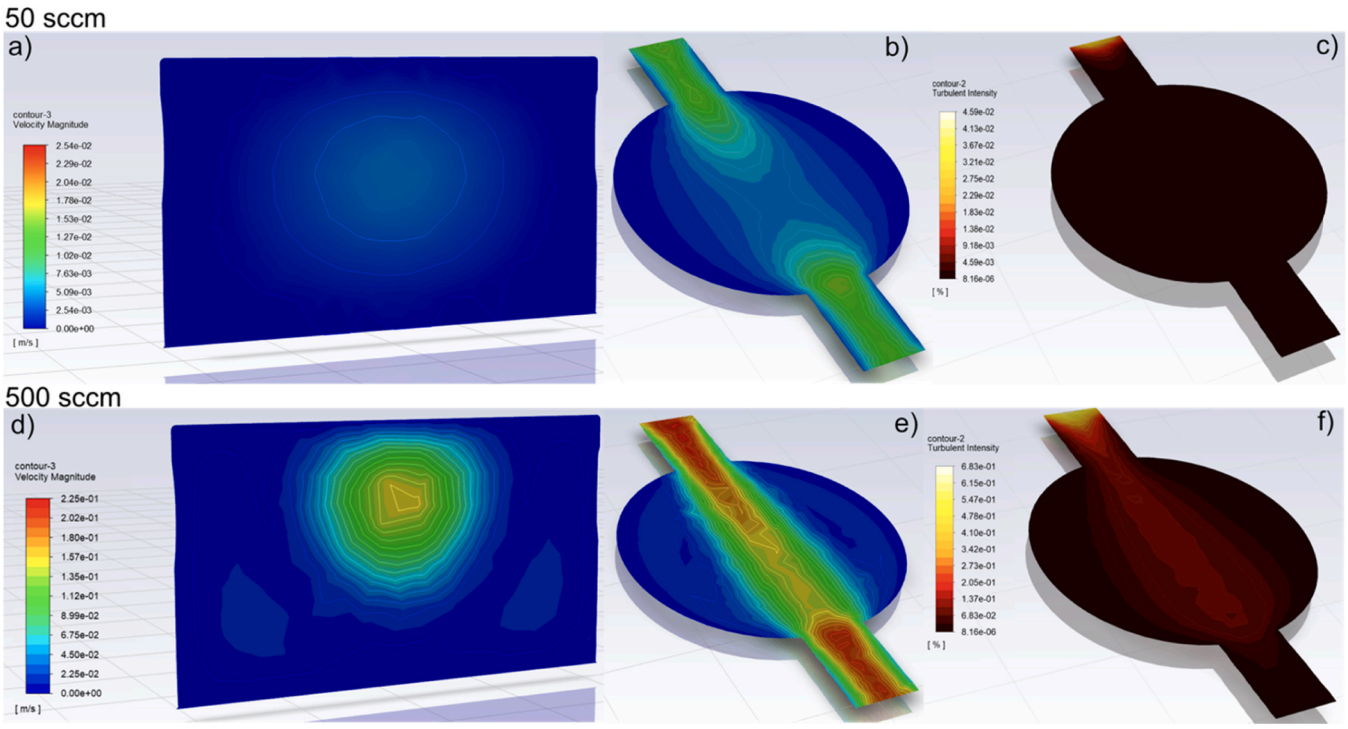

Fig. 5. Flow Field magnitude on a plane perpendicular to inlet and outlet and placed at the center of the chamber simulated at MFR of 50 sccm (a) and 500 sccm (d). Flow Field magnitude ((b) and (e)) and turbulent intensity ((c) and (f)) on the plane represented by the horizontal section containing the axis of inlet and outlet, at 50 sccm ((b) and (c)) and 500 sccm ((e) and (f)) MFRs.

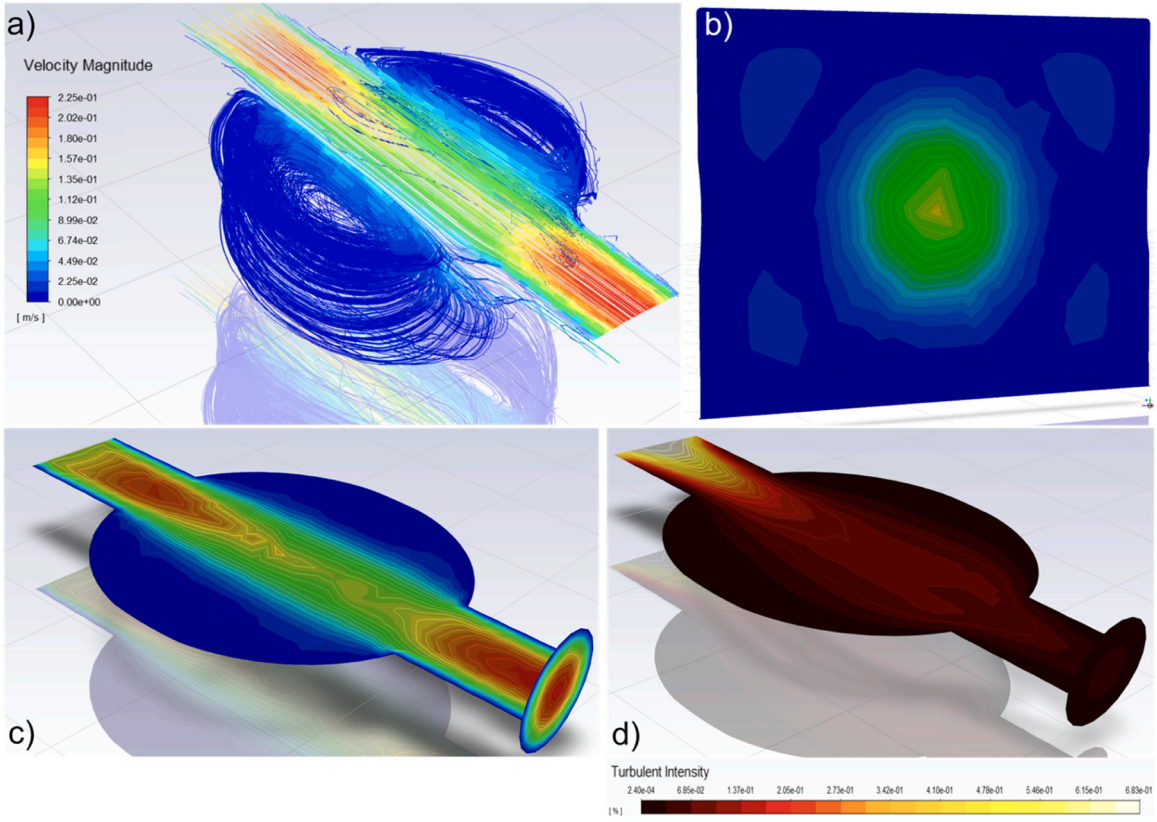

Fig. 6. Flow Field analysis at 500 sccm in ADM02 within the empty volume chamber (a); flow field magnitude on a plane perpendicular to inlet and outlet and placed at the center of the chamber (b) and on the plane cutting the center of inlet and outlet (c); turbulent intensity on the plane cutting the center of inlet and outlet (d).

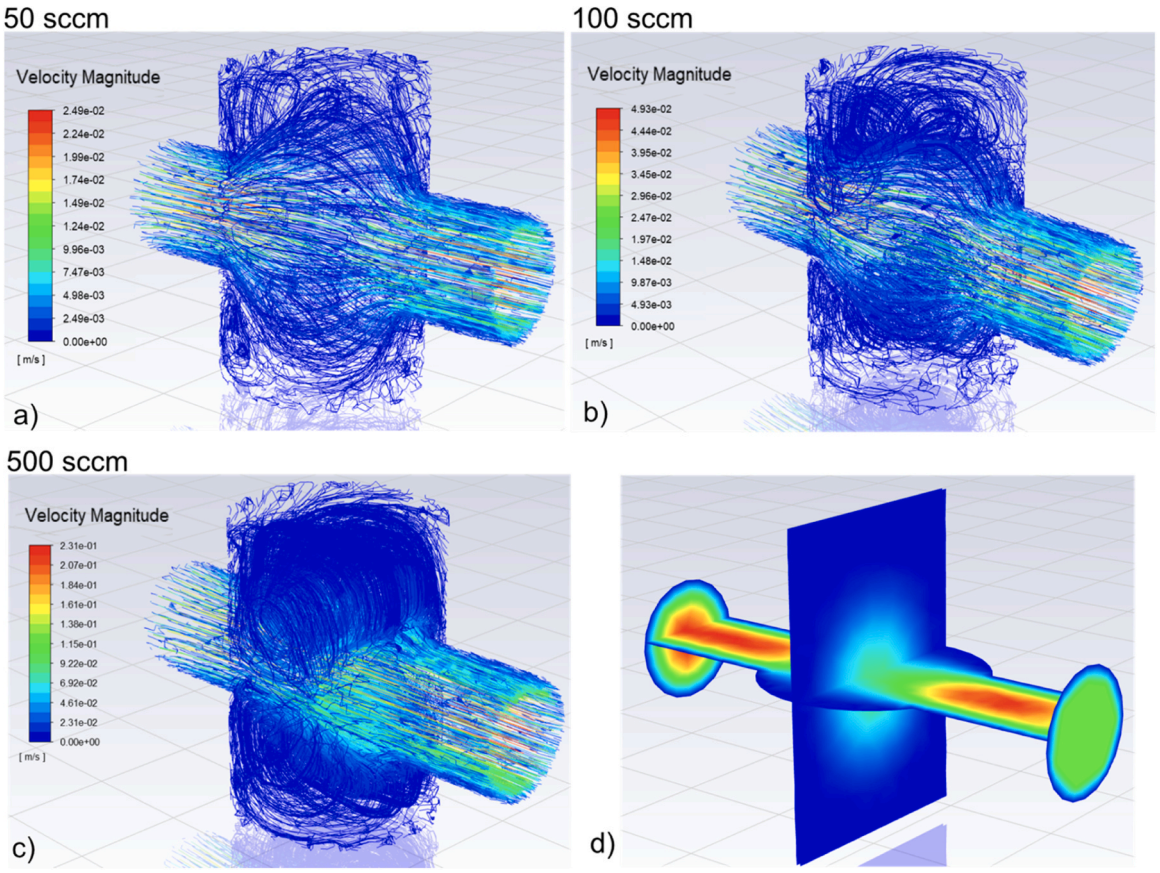

Fig. 7. Flow field analysis within the empty volume chamber of ADM03 at 50 sccm (a), 100 sccm (b), and 500 sccm (c). Flow field magnitude on a plane perpendicular to inlet and outlet and placed at the center of the chamber ADM03 at 500 sccm(d).

small regions above and below the mainstream with negligible vortices formation not affecting the mainstream (Fig. 7a). At 100 sccm, the occurrence of weak vortices can be observed. Being confined in a small space above and below the mainstream, the weak vortices do not lead to the formation of dead volumes (Fig. 7b). At 500 sccm, symmetric vortical regions appear above and below the mainstream. However, these vortices are completely formed, do not interact each other and converge towards the mainstream (Fig. 7c), namely they reinforce it, with a symmetric and homogenous distribution of the flow field magnitude on the plane perpendicular to inlet and outlet and placed at the center of the chamber (Fig. 7d). However, the volume below the mainstream is not empty because of the support for resonator tubes.

5. Experimental results

The influence of the gas turbulence on the performance of QEPAS sensing was investigated by assembling a QEPAS sensor with interchangeable volume chamber following the architecture depicted in Ref. [28], with a gas handling system reported in Fig. 3. An Interband Cascade Laser (ICL) with a central emission wavelength of 3345 nm was used as light source exciting the methane molecules within the ADM at 2988.8 cm^{-1}. The ICL current dynamic range is I = 15–70 mA and the optimal operating temperature range is T = 15 °C. The ICL is mounted in a standard TO66 package equipped with a collimating lens. The beam emerging from the lens has a nearly perfect Gaussian power distribution with a diameter of 3 mm. Both ADM01 and ADM02 accommodate a spectrophone SPH1 composed of a T-shaped QTF acoustically coupled with a pair of resonator tubes [29]. The two tubes were mounted on both sides of the QTF at 200 μm, perpendicular to the QTF plane, and with the tube center 2 mm below the QTF top. Both tubes have a length of 12.4 mm, an internal and external diameter of 1.59 and 1.83 mm, respectively. The spectrophone SPH3 mounted inside ADM3 consists of a standard 32.7 KHz-QTF coupled with a pair of resonator tubes having a length of 4.4 mm and an internal diameter of 0.8 mm [30]. QEPAS measurements were performed operating the sensor in 2 f-wavelength modulation (2 f-WM). The laser injection current was modulated at half of the resonance frequency of the QTF while the electric signal generated by the spectrophone was demodulated at its resonance frequency by means of a lock-in amplifier, whose time constant was set at 0.1 s.

The pressure of the gas mixture flowing inside the ADM was regulated using a pressure controller (MKS Type 649), while the MFR was set by the flow controller (MCQ Instruments, Gas Blender 103) from 50 sccm to 500 sccm. The gas sample used for all measurements reported in this work is a certificated concentration of 50 part-per-million (ppm) of CH_4 in N_2.

5.1. Vacuum seal test

A vacuum seal test was performed for all the three ADMs to verifying that any potential external leak would not alter the measurements. Starting from the gas handling system reported in Fig. 3, the pressure controller was removed to be replaced by a pressure meter, and the vacuum pump turned on to reach the minimum possible value of the pressure inside the ADM. Then, the pump was isolated, and the pressure value monitored for 10 minutes. The results are reported in Fig. 8 for all three ADMs.

Results clearly show how the three seal curves follow the same trend, meaning that potentially external leak cannot affect differently the three ADMs.

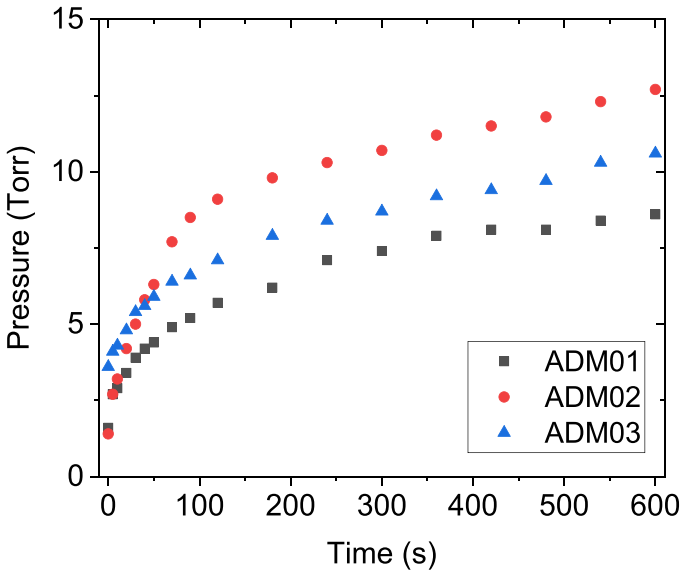

Fig. 8. The vacuum seal test for the three ADMs.

5.2. *Impact of high flow rates on spectrophone properties*

The use of high flow rates with the consequent formation of vortices and turbulences could impact the proper operation of the spectrophone even before influencing the generated QEPAS signal. This effect may occur in three ways: i) modification of the acoustic coupling between the QTF and the resonator tubes; ii) alteration of the resonance properties; and iii) deterioration of the noise level.

First, the acoustic coupling between the QTF and the resonator tubes was evaluated. At the highest flow rate (500 sccm), the molecules enter in the ADM with a velocity $v \sim 0.2$ m/s and reach the center of the ADM at roughly $\sim v/2$, as reported in the simulation results (see Fig. 4e as an example). Thus, the photoacoustic Doppler effect can occur: the intensity modulated light wave induces a photoacoustic wave on moving particles with a specific frequency f_0. The frequency f detected by the receiver due to the motion of the absorber differs from f_0, and it results:

$$f = \frac{v}{v + v_s} f_0 \tag{3}$$

where $v_s = 353$ m/s is the speed of sound in a nitrogen matrix. The frequency shift can affect the acoustic coupling between the QTF and the resonator tubes, deteriorating in turn the enhancement factor on the acoustic standing wave intensity within tubes: the calculation of the optimal tube length based on an open-end correction predicts its dependence on the tube radius and on the sound frequency in the system of moving molecules:

$$l = \frac{v_s}{2f_0} \quad -\frac{16a}{3\pi} \tag{4}$$

Considering the Doppler shift, the optimal tube length can be recalculated by replacing f_0 in Eq. (4) with the expression of f in Eq. (3). With $v = 0.1$ m/s (corresponding to 500 sccm), the correction of the tube length is less than 100 μm and 10 μm for SPH1 and SPH3, respectively, a value that is too low to significantly affect the coupling between the tubes and the QTF [30].

Second, the resonance properties of the spectrophone were determined by measuring both its resonance frequency and quality factor, at different flow rates. The laser emission wavelength was locked at the CH_4 absorption located at 2988.8 cm^{-1}. To reconstruct the resonance response curve of the spectrophone, the ICL current modulation frequency was varied step-by-step in the range 6228.4 Hz – 6230 Hz, half of the resonance frequency of the QTF, while the QEPAS sensor operated in 2 f-WM. The frequency response of SPH1 close to the fundamental mode is shown in Fig. 9a for ADM01 and four MFR values at 240 Torr.

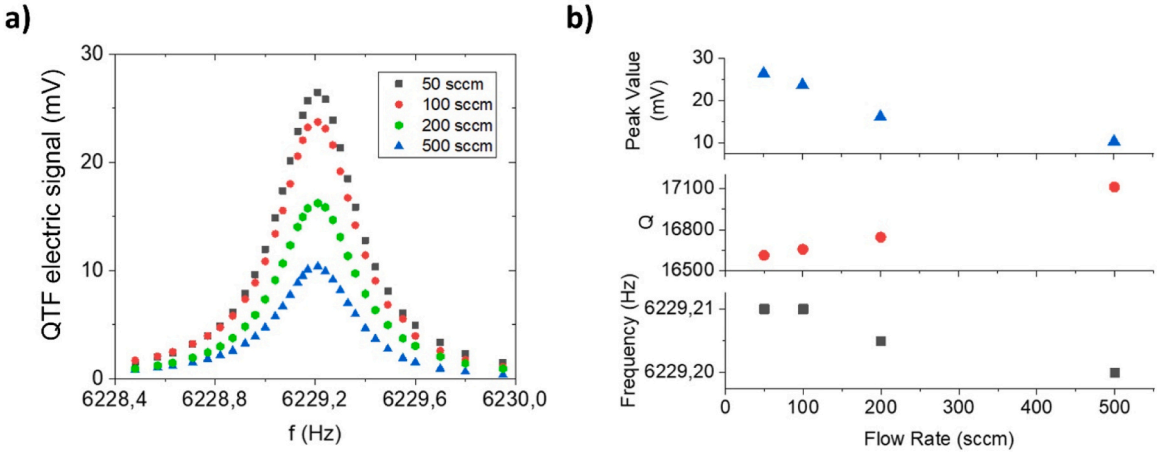

Fig. 9. a) Resonance curves of the spectrophone acquired via photoacoustic excitation in 2 f-WM with the laser source locked to the methane absorption peak, for different flow rates. b) Peak value, quality factor and resonance frequency extracted from each resonance curve and plotted as a function of the flow rate.

The peak values, the resonance frequency and the quality factor were extracted by imposing a Lorentzian fit to the experimental data and plotted as a function of the flow rate in Fig. 9b. Apart the decreases of the peak value that will be analyzed in the next section, negligible shifts of the resonance frequency and deterioration of the quality factor were observed as the flow rate increases, meaning that the resonance properties of the spectrophone are not significantly altered up to flow rates of 500 sccm.

Finally, the noise level of the QEPAS sensors at different flow rate was evaluated. Turbulences and instabilities may cause a deterioration of the ultimate noise level of the spectrophone. The QEPAS signal was acquired for more than one hour with a sampling rate of 0.3 s by locking the laser emission to the absorption peak of the CH_4 line, at different flow rates. The time-dependence QEPAS signal acquired with SPH1 in ADM01 is plotted in Fig. 10 for the investigated MFRs, namely 50, 100, 200 and 500 sccm, at 240 Torr.

The noise level was estimated as 1σ standard deviation of signal fluctuations, resulting in ~ 0.16 mV for all four flow rates. Higher MFR does not generate higher level of noise: the QTF thermal noise is the only noise source even with flow rates as high as 500 sccm. A drift of the QEPAS signal over time is observed. Several phenomena contribute to compromise the long-term stability of the QEPAS signal, mainly the laser intensity fluctuations and the slow mechanical vibrations affecting the acoustic detection module [31]. However, results reported in Fig. 10 show a signal drift less than ~3 % of the mean value in the worst case, i.e., at 100 sccm. This fluctuations level has a negligible impact on the QEPAS signal analysis with respect to the effect caused by the flow field distribution, as will be discussed in the next session.

The results demonstrated regarding the measurement of resonance properties and noise level, respectively, were also verified for SPH1 mounted in ADM02 and SPH3 mounted in ADM03.

5.3. *Influence of the mass flow rate on the QEPAS Signal*

Fig. 11 shows the QEPAS signal at different MFRs, normalized to the QEPAS signal acquired at 50 sccm, for ADM01 and ADM02, at three different pressures: 240 Torr, 400 Torr, and 700 Torr.

At a fixed pressure value, the performance of the QEPAS sensor clearly deteriorates as the MFR increases both for ADM01 and ADM02, especially for the lowest pressure value (240 Torr). The flow field analysis demonstrated that the flow field significantly widens and spread from the mainstream as the flow rate increases (see Figs. 5e and 6c). Moreover, the formation of lateral vortices weakens the mainstream. The spatial density of the velocity field roughly retraces the spatial distribution of the molecules within the ADM. As a result, both effects lead to a lower number of molecules reaching the center the ADM, where the spectrophone is placed, as the flow rate increases. Thus, the absolute number of nitrogen molecules is reduced as well as that of target molecules, with respect to the case with no vortices. However, the concentration of absorbing molecules, namely the ratio between the absorbing molecules and the nitrogen molecules, remains unaltered. This because the separation of the molecules from the mainstream does not represent a selective inertial sorting of the two different types of molecules. Both reductions negatively affect the photoacoustic wave generation, but in a different manner. A lower density of molecules negatively affects the photoacoustic wave generation in two consequential manners: first, a lower number of absorbing molecules reduces the local heat generation; then, the reduced number as well as a spatial non-uniformity of the nitrogen molecules composing the matrix compromises the efficiency of sound wave generation. At 240 Torr, the situation for ADM02 is even worse. Even simulations demonstrated that the flow field is fully developed on the center plane of the device, so that vortices can reinforce the mainstream on this plane (see Fig. 6a), double the number of dead zones with respect to ADM01 (from 2 for ADM01 to 4 for ADM01, Fig. 5d to be compared with Fig. 6b) and have been no beneficial for the ultimate sensor performance. Results clearly show that the QEPAS signal vs flow rate-dependence is strongly reduced in ADM03, supporting the conclusion drawn from the modeling analysis, namely the reduced radius of the chamber inhibits the formation of lateral vortices which in turn reduce the impact on the QEPAS signal. Moreover, the results reported in Fig. 11 support the conclusion that the effect of MFR on QEPAS signal is dependent on the spatial distribution of molecules, as the signal worsening is the highest at 240 Torr (up to ~70 % reduction) and decreases as the pressure increases to 700 Torr (up to 30 % reduction)

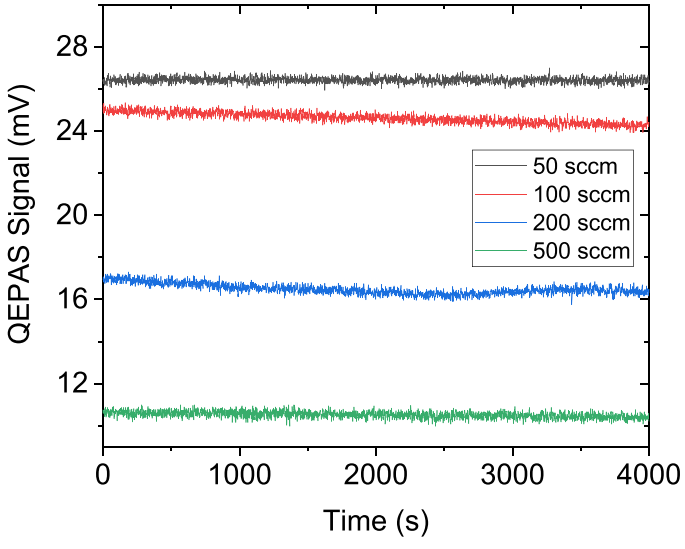

Fig. 10. QEPAS signal as a function of time acquired with ADM01 at different flow rates at 240 Torr.

For all the three chambers, the dependence of the QEPAS signal on the flow rate is less pronounced increasing the pressure. In particular, with ADM03 the QEPAS signal decreases of only 6 % when the flow rate passes from 50 to 500 sccm at nearly atmospheric pressure (700 Torr). This behavior is strictly related to the operating conditions. While the MFR and the injection conditions determine the velocity field distribution (and so the spatial distribution of molecules) within the chamber as well as regulate the rapidity of gas exchange from inlet to outlet, the pressure controller fixes the total number of molecules remaining in the cell per unit of time. As a result, the increase of the pressure reinforces the population of the mainstream as much as vortices. This is expected to produce strong evidence in the cases with significant vortices (high flow rates): when the spatial density of molecules is low, a slight local increase of the molecular density nearby the photoacoustic source point can generate a huge beneficial for QEPAS efficiency because of a more efficient pumping of non-radiative channels for the vibrational-to-translation energy conversion. This is similar to the typical dependence of QEPAS signal as a function of the pressure: as the pressure increases, the QEPAS signal sharply reaches the maximum value; conversely, beyond this value, it slightly decreases [32,33].

6. Conclusions

In this work, we investigated the impact of high MFRs on the performance of a QEPAS sensor. The MFRs typically employed for sensing applications were evaluated, comparing the sensor's response in different experimental conditions. First, numerical simulations were set to determine the flow field distributions in three ADMs with different geometries. Then, the theoretical results were used to validate experimental measurements performed at different MFRs and at different operating pressure. With large volume chambers and high MFRs, vortices formation is inevitable, generating dead volumes on the corners, as confirmed by the simulation results for the two largest volume

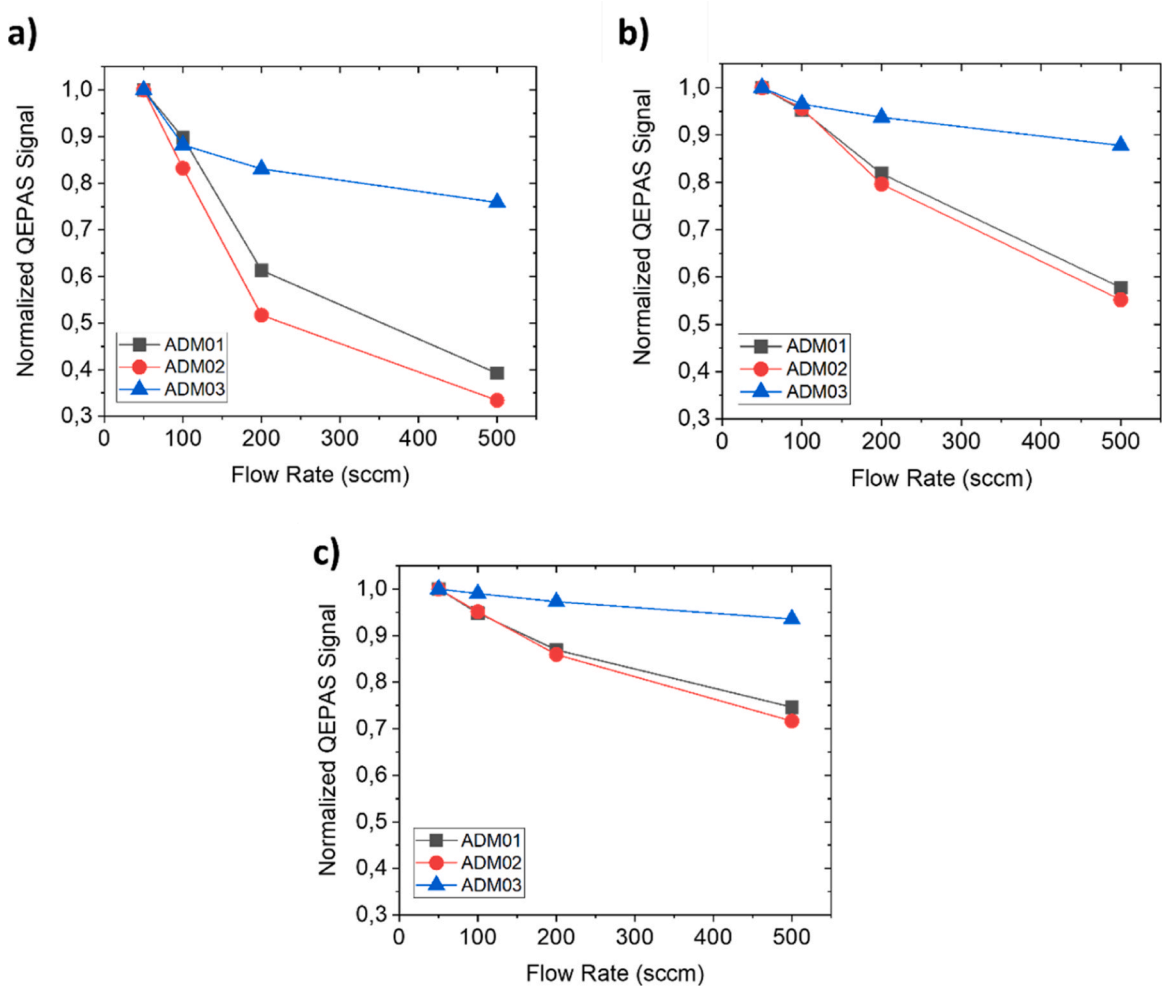

Fig. 11. Normalized QEPAS signals acquired at different flow rates with an operating pressure of (a) 240 Torr; (b) 400 Torr; and (c) 700 Torr. The straight line connecting the data points are guides to the eye.

chambers. However, the experimental results demonstrated that increasing the MFR up to 500 sccm does not impact on the proper operation of the spectrophone as its resonance properties and noise level remain unaltered. Thus, the decrease of the QEPAS signal as MFR increases must be found in the analysis of the flow field distribution within the gas chamber. The investigation performed combining a computational approach and an experimental analysis points out that the deterioration of QEPAS signal at high MFRs is due to dead volumes created by vortices. Both the formation of eddies and the widening of the mainstream reduce the number of absorbing molecules hitting the spectrophone, altering the efficiency of photoacoustic generation. The analysis performed in this work highlights how shrinking the volume of the gas chamber suppresses the formation of lateral vortices, thus strongly reducing the dependence of the QEPAS signal on MFR. However, the choice of the best geometry provided by the results of the simulation must also face out with the complexity of fabrication process of the acoustic detection module. Volumes without sharp edges properly designed to accommodate the widening of the mainstream, i.e., an oval geometry, would be beneficial for the vortex's suppression. However, the fabrication process of the volume chamber would become more and more complex, and its final cost would increase as well. Therefore, our guideline is to relate the volume chamber to the specific application. For gas sensing applications requiring operation at high flow rates, minimizing the internal volume of the ADM chamber is the only way to reduce the dependence of the QEPAS signal on the flow rate at the inlet of the gas chamber, at a cost of more complex fabrication and hard optical alignment. Conversely, for gas sensing applications requiring operation at low flow rates, larger volume can be exploited, benefiting from easier optical alignment and simpler fabrication processes.

Fundings

This work was supported by National Natural Science Foundation of China (NSFC) (Nos. 62122045, 62075119, 62235010, 62175137); National Key R&D Program of China, code: 2019YFE0118200; The High-end Foreign Expert Program (Nos. G2023004005L); The Shanxi Science Fund for Distinguished Young Scholars (20210302121003). The authors from Dipartimento Interateneo di Fisica di Bari acknowledge financial support from Project PNC 0000001 D3–4Health Digital Driven Diagnostics, prognostics and therapeutics for sustainable Health care - CUP [B83C22006120001], The National Plan for Complementary Investments to the NRRP, Funded by the European Union - NextGenerationEU and National Recovery and Resilience Plan (NRRP), project "BRIEF—Biorobotics Research and Innovation Engineering Facilities", Mission 4: "Istruzione e Ricerca", Component 2: "Dalla ricerca all'impresa", Investment 3.1: "Fondo per la realizzazione di un sistema integrato di infrastrutture di ricerca e innovazione", CUP: J13C22000400007, funded by European Union—NextGenerationEU. The authors from PolySenSe Lab acknowledge financial support from project EVOQUE - "ENHANCED SELECTIVITY VOC DETECTION USING NOVEL GC-QEPAS" - HORIZON-CL4–2023-DIGITAL-EMERGING-01 - Grant Agreement Project n. 101135764.

CRediT authorship contribution statement

Giuseppe Negro: Writing – review & editing, Methodology, Formal analysis, Data curation, Conceptualization. **Lavinia Anna Mongelli:** Writing – review & editing, Investigation, Formal analysis, Data curation. **Andrea Zifarelli:** Writing – review & editing, Writing – original draft, Investigation, Data curation, Conceptualization. **Angelo Sampaolo:** Writing – review & editing, Resources, Investigation. **Ezio Ranieri:** Writing – review & editing, Data curation. **Lei Dong:** Writing – review & editing, Data curation. **Giuseppe Gonnella:** Writing – review & editing, Supervision, Methodology. **Vincenzo Luigi Spagnolo:** Writing – review & editing, Investigation, Funding acquisition, Formal analysis, Conceptualization. **Hongpeng Wu:** Writing – review & editing, Resources, Funding acquisition, Formal analysis, Data curation. **Pietro Patimisco:** Writing – review & editing, Writing – original draft, Methodology, Investigation, Funding acquisition, Formal analysis, Data curation, Conceptualization.

Declaration of Competing Interest

The authors declare that they have no known competing financial interests or personal relationships that could have appeared to influence the work reported in this paper.

Data availability

Data will be made available on request.

References

[1] A. Dey, Semiconductor metal oxide gas sensors: A review, Mater. Sci. Eng. B. 229 (2018) 206–217.
[2] L. Capelli, S. Sironi, R. Del Rosso, Electronic noses for environmental monitoring applications, Sensors 2014 14 (2014) 19979–20007.
[3] X. Liu, S. Cheng, H. Liu, S. Hu, D. Zhang, H. Ning, A survey on gas sensing technology, Sens. (Switz.) 12 (2012) 9635–9665.
[4] S. Feng, F. Farha, Q. Li, Y. Wan, Y. Xu, T. Zhang, H. Ning, Rev. Smart Gas. Sens. Technol., Sens. 19 (2019) 3760.
[5] D.J. Wales, J. Grand, V.P. Ting, R.D. Burke, K.J. Edler, C.R. Bowen, S. Mintova, A. D. Burrows, Gas sensing using porous materials for automotive applications, Chem. Soc. Rev. 44 (2015) 4290–4321.
[6] Y. Liu, J. Parisi, X. Sun, Y. Lei, Solid-state gas sensors for high temperature applications – a review, J. Mater. Chem. A. 2 (2014) 9919–9943.
[7] C. Di Natale, R. Paolesse, E. Martinelli, R. Capuano,.
[8] S. Das, M. Pal, Non-Invasive Monitoring of Human Health by Exhaled Breath Analysis: A Comprehensive Review, J. Electrochem. Soc. 167 (2020) 037562.
[9] J. Hodgkinson, R.P. Tatam, Optical gas sensing: a review, Meas. Sci. Technol. 24 (2013) 012004.
[10] H.E. Joe, H. Yun, S.H. Jo, M.B.G. Jun, B.K. Min, A review on optical fiber sensors for environmental monitoring, Int. J. Precis. Eng. Manuf. Technol. 51 (5) (2018) 173–191.
[11] C.S. Goldenstein, R.M. Spearrin, J.B. Jeffries, R.K. Hanson,.
[12] B. Henderson, A. Khodabakhsh, M. Metsälä, I. Ventrillard, F.M. Schmidt, D. Romanini, G.A.D. Ritchie, S. te Lintel Hekkert, R. Briot, T. Risby, N. Marczin, F. J.M. Harren, S.M. Cristescu, Laser spectroscopy for breath analysis: towards clinical implementation, Appl. Phys. B Lasers Opt. 124 (2018) 1–21.
[13] N.W. Ryan, M.M. Johnson, Transistion from laminar to turbulent flow in pipes, AIChE J. 5 (1959) 433–435.
[14] V. Mukund, B. Hof, The critical point of the transition to turbulence in pipe flow, J. Fluid Mech. 839 (2018) 76–94.
[15] H. Hattori, A. Wada, M. Yamamoto, H. Yokoo, K. Yasunaga, T. Kanda, K. Hattori, Experimental study of laminar-to-turbulent transition in pipe flow, Phys. Fluids 34 (2022) 34115.
[16] B. Fu, C. Zhang, W. Lyu, J. Sun, C. Shang, Y. Cheng, L. Xu,.
[17] K. Krzempek, A Review of Photothermal Detection Techniques for Gas Sensing Applications, Appl. Sci. 9 (2019) 2826.
[18] F. Yang, Z. Li, W. Ren, Z. Wang, W. Jin, Mid-infrared fiber-optic photothermal interferometry, Opt. Lett. 42 (2017) 3718–3721.
[19] S. Palzer, Photoacoustic-based gas sensing: a review, Sensors 2020 20 (2020) 2745.
[20] K. Liu, J. Mei, W. Zhang, W. Chen, X. Gao, Multi-resonator photoacoustic spectroscopy, Sens. Actuators B Chem. 251 (2017) 632–636.
[21] T. Tomberg, M. Vainio, T. Hieta, L. Halonen, Sub-parts-per-trillion level sensitivity in trace gas detection by cantilever-enhanced photo-acoustic spectroscopy, Sci. Rep. 8 (2018) 1848.
[22] Y. Yin, D. Ren, C. Li, R. Chen, J. Shi, Cantilever-enhanced photoacoustic spectroscopy for gas sensing: A comparison of different displacement detection methods, Photoacoustics 28 (2022) 100423.
[23] S. Qiao, Y. He, H. Sun, P. Patimisco, A. Sampaolo, V. Spagnolo, Y. Ma, Ultra-highly sensitive dual gases detection based on photoacoustic spectroscopy by exploiting a long-wave, high-power, wide-tunable, single-longitudinal-mode solid-state laser, Light Sci. Appl. 13 (2024) 1–16.
[24] Y. Ma, Review of Recent Advances in QEPAS-Based Trace Gas Sensing, Appl. Sci. 8 (2018) 1822.
[25] A. Sampaolo, P. Patimisco, M. Giglio, A. Zifarelli, H. Wu, L. Dong, V. Spagnolo, Quartz-enhanced photoacoustic spectroscopy for multi-gas detection: A review, Anal. Chim. Acta 1202 (2022) 338894.
[26] T. Liang, S. Qiao, Y. Chen, Y. He, Y. Ma, High-sensitivity methane detection based on QEPAS and H-QEPAS technologies combined with a self-designed 8.7 kHz quartz tuning fork, Photoacoustics 36 (2024) 100592.
[27] THORLABS ADM01 ⟨https://www.thorlabs.com/newgrouppage9.cfm?objectgroup_id=2940⟩, (n.d.).
[28] P. Patimisco, N. Ardito, E. De Toma, D. Burghart, V. Tigaev, M.A. Belkin, V. Spagnolo, Quartz-Enhanced Photoacoustic Sensor Based on a Multi-Laser Source for In-Sequence Detection of NO2, SO2, and NH3, Sensors 23 (2023) 9005.
[29] P. Patimisco, A. Sampaolo, M. Giglio, S. Dello Russo, V. Mackowiak, H. Rossmadl, A. Cable, F.K. Tittel, V. Spagnolo, Tuning forks with optimized geometries for quartz-enhanced photoacoustic spectroscopy, Opt. Express 27 (2019) 1401.
[30] S. Dello Russo, M. Giglio, A. Sampaolo, P. Patimisco, G. Menduni, H. Wu, L. Dong, V.M.N. Passaro, V. Spagnolo, Acoustic coupling between resonator tubes in quartz-enhanced photoacoustic spectrophones employing a large prong spacing tuning fork, Sens. (Switz.) 19 (2019).
[31] M. Giglio, P. Patimisco, A. Sampaolo, G. Scamarcio, F.K. Tittel, V. Spagnolo, Allan Deviation Plot as a Tool for Quartz-Enhanced Photoacoustic Sensors Noise Analysis, IEEE Trans. Ultrason. Ferroelectr. Freq. Control. 63 (2016) 555–560.
[32] T. Milde, M. Hoppe, H. Tatenguem, M. Mordmüller, J. O'Gorman, U. Willer, W. Schade, J. Sacher, QEPAS sensor for breath analysis: a behavior of pressure, Appl. Opt. 57 (2018) C120.
[33] M. Olivieri, A. Zifarelli, G. Menduni, M. Di Gioia, C. Marzocca, V.M.N. Passaro, A. Sampaolo, M. Giglio, V. Spagnolo, P. Patimisco, Influence of air pressure on the resonance properties of a t-shaped quartz tuning fork coupled with resonator tubes, Appl. Sci. 11 (2021) 7974.

Andrea Zifarelli received the M.S. degree (cum laude) in Physics in 2018 from the University of Bari and his Ph.D. in Physics from the same institution in 2022. His research activities were mainly focused on the development of spectroscopic techniques based on laser absorption for the analysis of complex gas mixtures by employing quartz tuning forks as sensitive elements. This investigation was performed by using innovative laser sources as well as developing new algorithms for multivariate analysis approaches. Currently, he is Research Associate at University of Bari and his research activities are carried out at the PolySenSe Lab, joint-research laboratory between Technical University of Bari and THORLABS GmbH.

Lavinia Anna Mongelli obtained her M.S. degree in Physics in 2024 from the University of Bari. Currently she is research fellow at the Physics Department of the University of Bari, developing her research work at PolySense Lab, joint-research laboratory between Technical University of Bari and THORLABS GmbH. Her research activities are focused on the development of gas sensors based on optical spectroscopy for the detection of Volatile Organic Compounds and other gas species of interest for environmental and human health monitoring.

Angelo Sampaolo obtained his Master degree in Physics in 2013 and the PhD Degree in Physics in 2017 from University of Bari. He was an associate researcher in the Laser Science Group at Rice University from 2014 to 2016 and associate researcher at Shanxi University since 2018. Since 2019, he is Assistant Professor at Polytechnic of Bari. His research activity has focused on the development of innovative techniques in trace gas sensing, based on Quartz-Enhanced Photoacoustic Spectroscopy and covering the full spectral range from near-IR to THz.

Lei Dong received his Ph.D. degree in optics from Shanxi University, China, in 2007. From June, 2008 to December, 2011, he worked as a post-doctoral fellow in the Electrical and Computer Engineering Department and Rice Quantum Institute, Rice University, Houston, USA. Currently he is a professor in the Institute of Laser Spectroscopy of Shanxi University. His research interests include optical sensors, trace gas detection, photoacoustic spectroscopy and laser spectroscopy.

Hongpeng Wu received his Ph.D. degree in atomic and molecular physics from Shanxi University, China, in 2017. From September, 2015 to October, 2016, he studied as a joint Ph.D. student in the Electrical and Computer Engineering Department and Rice Quantum Institute, Rice University, Houston, USA. Currently he is a professor in the Institute of Laser Spectroscopy of Shanxi University. His research interests include gas sensors, photoacoustic spectroscopy, photothermal spectroscope and laser spectroscopy techniques.

Prof. Pietro Patimisco obtained the Master degree in Physics (cum laude) in 2009 and the PhD Degree in Physics in 2013 from the University of Bari. Since 2023, he is an associate professor at the Physics Department of University of Bari. He was a visiting scientist in the Laser Science Group at Rice University in 2013 and 2014. The main scientific skills of Pietro Patimisco are related to the development of spectroscopic techniques for studying the light-matter interaction in the infrared range. Prof. Pietro Patimisco is co-founder of "PolySenSe Innovations", a company devoted to the development of optical-based sensors.

Spagnolo Vincenzo received the degree (summa cum laude) and the PhD, both in physics, from University of Bari. He works as Full Professor of Applied Physics at the Technical University of Bari. In 2019, he become Vice-Rector of the Technical University of Bari, deputy to Technology Transfer. Since 2017, he is the director of the joint-research lab PolySense, created by THORLABS GmbH and Technical University of Bari, devoted to the development and implementation of novel gas sensing techniques and the realization of highly sensitive QEPAS trace-gas sensors.

Giuseppe Negro developed his academic career in non-equilibrium statistical physics and soft matter, focusing on complex and active fluids. After obtaining a Ph.D. at the University of Bari(Italy) on the modelization and simulations of active fluids, he continued to work on complex fluids with theory and simulations at the University of Edinburgh. In particular, he discovered two new types of quasi-two-dimensional topological phases: finite quasicrystals and amorphous structures, both made up of mixtures of polygonal tessellations of half skyrmions. Currently, he is pursuing his research as an independent researcher at the University of Bari, focusing on strategies to control flows and topology of active emulsions.

Prof. Giuseppe Gonnella has been a Full Professor in the scientific-disciplinary sector "FIS/02 Theoretical Physics, Models, and Mathematical Methods" at the Department of Physics of the University of Bari "Aldo Moro" since 2018, where he has held various managerial roles over the years. After earning his Phd in Physics at the University of Bari, he moved to Oxford as a Postdoc in the group of Julia Yeomans, where he studied phase field and numerical models of complex fluids. He is currently the coordinator of the Ph.D. program in Physics. His research activity is mainly in the field of statistical mechanics and focuses on the development of theoretical descriptions of non-equilibrium phenomena, the study of fluids with phase transitions, the modeling of biological systems, complex fluids, and active matter.